Pergamon

Tetrahedron: *Asymmetry* 10 (1999) 265–279

TETRAHEDRON: *ASYMMETRY*

Computational study of solvation and stereoselectivity in deprotonation of cyclohexene oxide by a chiral lithium amide

Sten O. Nilsson Lill, Per I. Arvidsson and Per Ahlberg *

Organic Chemistry, Department of Chemistry, Göteborg University, SE-412 96, Göteborg, Sweden

Received 10 November 1998; accepted 14 December 1998

Abstract

A detailed computational investigation of possible activated complexes in the epoxide opening of cyclohexene oxide by a chiral lithium amide is presented. Transition states for the two routes giving (*S*)- and (*R*)-alkoxides with and without solvent have been calculated. Geometry optimizations at PM3 and HF/3-21G levels of theory, and single point calculations at B3LYP/6-31+G(d) level have been used. The experimentally obtained stereoselectivity is semi-quantitatively reproduced at all levels except PM3//PM3. The factors found to control the stereoselectivity are solvation and some non-bonded interactions other than those previously proposed. © 1999 Elsevier Science Ltd. All rights reserved.

1. Introduction

Enantioselective deprotonation of *meso*-epoxides by chiral lithium amides yielding chiral allylic alcohols in high yield and enantiomeric excess (e.e.) is of increasing importance in synthesis. There are many recent reports on improvement of the stereoselectivity and yield obtained by trial and error structural changes of the amides.[1–26] Surprisingly, no thorough experimental or theoretical studies of the epoxide opening mechanism and initial- and transition-state structures can be found in the literature. Thus the basis for rational design of effective stereoselective amides is lacking.

The challenge to predict and interpret the stereoselectivity in lithium organic chemistry computationally has recently been accepted by a few groups.[27–30] Major questions to be answered concern the structures and energies of transition states (TS) and the role of solvation. However, the task is difficult due to the complexity of the systems.

Following our previous reports,[19,31–34] which include solvent effects on enantioselective deprotonation of epoxide and solvent induced isomerization of allylic alcohol to homoallylic alcohol, we now

* Corresponding author. Tel: +46-31-772-2899; fax: +46-31-772-2908; e-mail: per.ahlberg@oc.chalmers.se

PII: S0957-4166(98)00501-1

present a computational study of the epoxide opening of cyclohexene oxide (**1**) by lithium (*S*)-(+)-2-(1-pyrrolidinylmethyl)-pyrrolidide (**2**) which predicts the observed stereoselectivity and indicates the origin of the stereoselectivity. In particular the important role of the solvent, i.e. THF (Fig. 1), is demonstrated. Our study is limited to complexes between monomeric lithium amide and epoxide although oligomers of the base may be reactive and contribute to the product formation.

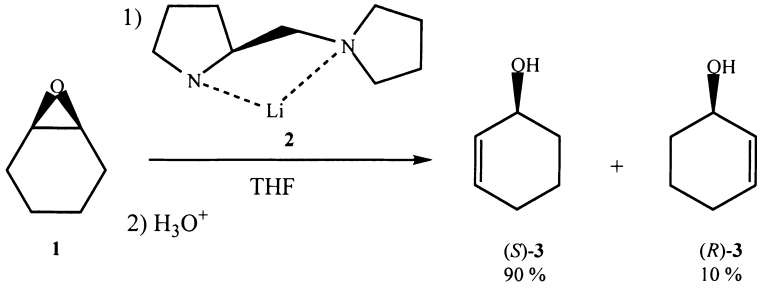

Figure 1. Epoxide opening of cyclohexene oxide (**1**) with the chiral lithium amide **2** yielding the allylic alcohols (*S*)-**3** and (*R*)-**3**

2. Computational methods

All ab initio calculations were performed using the Gaussian 94[35] program, while semiempirical calculations were done using the Spartan[36] program. Geometries were optimized at PM3[37,38] and HF/3-21G[39] levels of theory. At the PM3 level, the option HHON in Spartan was used to correct for hydrogens in close contact.[40,41] Due to the size of the studied system no TS optimizations have been performed at higher levels. All geometries were characterized as minima or transition states on the potential energy surface (PES) by use of the sign of the eigenvalues of the force constant matrix obtained from a frequency calculation. Calculated transition states with one imaginary frequency were confirmed to describe the correct displacement on the PES by a mode analysis. Reaction energies and activation barriers are calculated at PM3, HF/3-21G, and B3LYP/6-31+G(d)[42–44] levels of theory.

3. Results and discussion

Amide promoted β-elimination of cyclohexene oxide yielding an allylic alcohol was shown in deuterium labeling experiments by Thummel and Rickborn,[45] and later by Morgan and Gajewski,[20] to take place exclusively *syn* to the oxygen. The epoxide and lithium amide were suggested to form a 1:1 monomeric complex in which the deprotonation takes place.

Cyclohexene oxide can rapidly isomerize between two chiral enantiomeric half-chair conformations (Scheme 1). An activation barrier of 4.2 kcal mol^{-1} of this isomerization was calculated at the PM3 level, which is to be compared with the experimental value of 4.3 kcal mol^{-1}.[46]

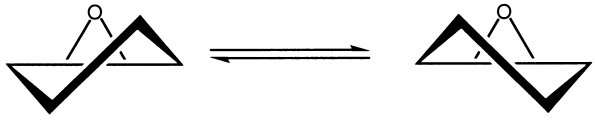

Scheme 1.

The lithium amide **2** will react with both enantiomers and form pre-complexes (**PC1** and **PC2**) in which the deprotonation takes place. The pre-complexes are presumably rapidly interconverting and the

transition states for (*R*)- and (*S*)-alkoxide, (**TS1** and **TS2**), respectively, are in equilibrium according to the Curtin–Hammett principle.[47,48] This means that the stereoselectivity is determined by the difference in free energy ($\delta\Delta G^{\ddagger}$) between the transition states, while the energies of the pre-complexes contribute to the determination of the rates of the two routes (Scheme 2).

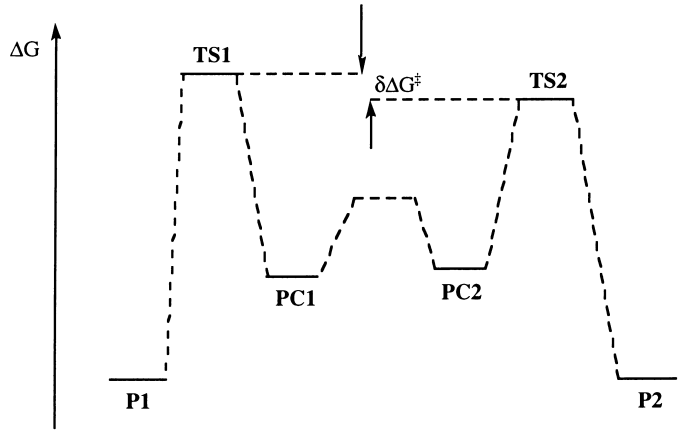

Scheme 2.

The epoxide opening reaction is found to be stereoselective (80% e.e. of (*S*)-alcohol)[15] and this represents a free energy difference between the diastereoisomeric transition states of 1.25 kcal mol^{-1} at 20°C.

Asami[5] rationalized the observed enantioselectivity by proposing that the deprotonation occurs preferentially through the transition state complex where the steric interactions between the cyclohexene oxide and the amide are minimized, i.e. **TS2**, leading to (*S*)-alcohol, is preferred over **TS1** (Fig. 2).

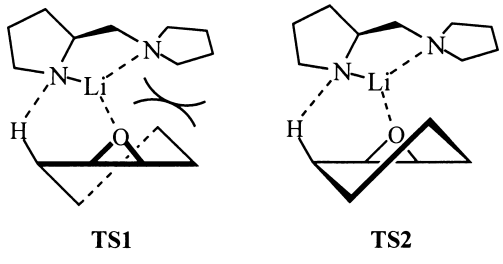

Figure 2. Proposed transition structures yielding (*R*)-alcohol (**TS1**) and (*S*)-alcohol (**TS2**)

3.1. Ab initio structures

Optimized transition states for the epoxide opening are presented in Fig. 3. Selected calculated bond distances of the optimized structures are given in Table 1.

At the HF/3-21G level, three transition states yielding the (*R*)-alkoxide (**TS1a**–**c**) and three yielding the (*S*)-alkoxide (**TS2a**–**c**) were identified. These TSs all have six-membered rings with Li coordinating to the epoxide oxygen (Scheme 3).

The epoxide opening is concerted with the proton abstraction, which is performed by the amidic nitrogen (N_2). In **TS1a**–**b** and **TS2c** the lithium amide is coordinated above the cyclohexene oxide ring while in **TS2a**–**b** and **TS1c** the amide is positioned outside the cyclohexene oxide ring.

At the HF/3-21G level, the epoxide ring is opened to nearly the same extent in **TS1** and **TS2**. O–C_1 distances are calculated to be 1.58–1.65 Å and O–C_6 distances are 1.47–1.48 Å. These are to be compared

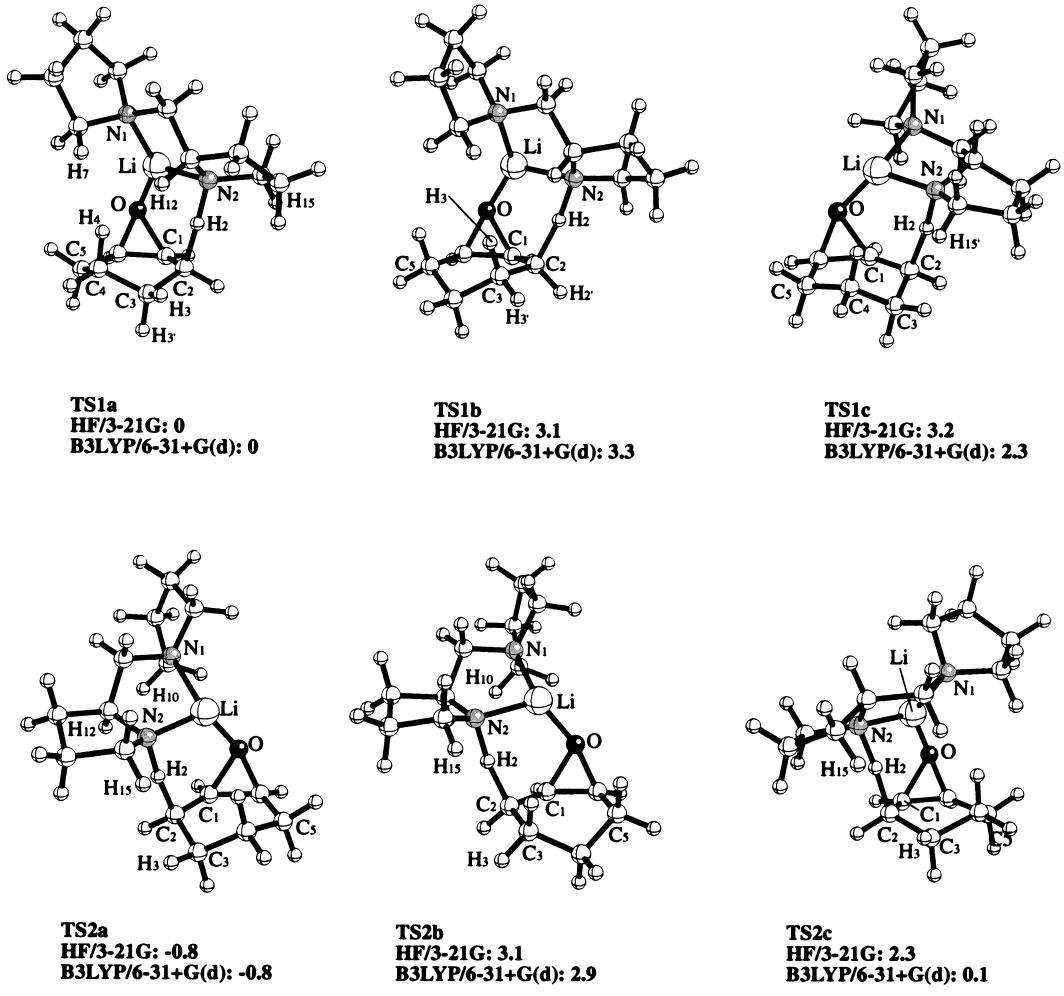

Figure 3. Calculated TSs for epoxide opening of cyclohexene oxide with **2** yielding (*R*)-alkoxide (**TS1a**–**c**) and (*S*)-alkoxide (**TS2a**–**c**)

with the O–C_1 and O–C_6 distances in cyclohexene oxide (**1**) which are calculated to be 1.48 Å, and the corresponding O–C bond distance in the lithium alkoxide of cyclohexen-2-ol (**3**) which is calculated to be 1.40 Å at the same level of theory. This suggests that the O–C_1 bond in the epoxide ring is partially broken in the transition state, while the O–C_6 bond is essentially unchanged. The double bond character is not fully developed between C_1 and C_2 as the bond distance is calculated to be 1.46–1.47 Å, and the hybridization at C_2 is in between sp^2 and sp^3. In **3**, with the double bond fully developed, the bond length is calculated at the same level of theory to be 1.32 Å. Abstraction of the proton in **TS1** and **TS2** is almost linear; the C_2–H_2–N_2-angle is calculated to be 171–173°. The proton is found to be more than half-transferred to the nitrogen; C_2–H_2 bonds are found to be 1.43–1.47 Å and N_2–H_2 bonds are 1.26–1.30 Å. The C_2–N_2 distances are calculated to be 2.72–2.78 Å, indicating the presence of strong hydrogen bonds. The reaction is dominated by proton transfer in the initial part of the reaction coordinate, while the epoxide opening is dominating in the later. Upon epoxide opening the developed oxyanion yields increased attraction by the lithium cation; O–Li distances are calculated to be 1.78–1.79 Å. The lithium cation is also coordinating the amide nitrogen, N_2, with a distance of 1.92 Å and the amine nitrogen, N_1, at distances of 2.02–2.08 Å. Thus the lithium cation is tricoordinated.

Table 1
Selected calculated bond distances (Å) for deprotonation transition states and comparable compounds at PM3 and HF/3-21G levels of theory

	Method	O-C_1	O-C_6	C_1-C_6	C_1-C_2	C_2-H_2	N_2-H_2	C_2-N_2	O-Li	Li-N_2	Li-N_1
1	PM3	1.439	1.435	1.494	1.513						
	HF/3-21G	1.480	1.471	1.477	1.515						
3	PM3		1.373	1.512	1.333				1.601		
	HF/3-21G		1.395	1.522	1.317				1.560		
TS1a	PM3	1.534	1.438	1.494	1.461	1.549	1.216	2.747	1.876	2.069	2.168
	HF/3-21G	1.636	1.468	1.469	1.460	1.438	1.293	2.722	1.779	1.918	2.034
TS1b	PM3	1.515	1.443	1.497	1.467	1.560	1.208	2.739	1.889	2.073	2.157
	HF/3-21G	1.584	1.483	1.473	1.474	1.474	1.262	2.723	1.788	1.922	2.028
TS1c	PM3	1.568	1.433	1.491	1.454	1.552	1.225	2.764	1.871	2.069	2.235
	HF/3-21G	1.639	1.467	1.469	1.460	1.459	1.298	2.749	1.781	1.917	2.083
TS1d	PM3	1.916	1.393	1.482	1.428	1.290	1.597	2.861	1.783	2.024	2.165
TS1e	PM3	1.887	1.398	1.481	1.430	1.346	1.559	2.884	1.780	2.026	2.166
TS1f	PM3	1.916	1.393	1.485	1.424	1.319	1.595	2.902	1.790	2.009	2.226
TS2a	PM3	1.541	1.437	1.493	1.460	1.545	1.222	2.753	1.880	2.065	2.172
	HF/3-21G	1.640	1.468	1.469	1.460	1.427	1.301	2.723	1.781	1.916	2.021
TS2b	PM3	1.541	1.438	1.493	1.460	1.546	1.224	2.748	1.859	2.069	2.175
	HF/3-21G	1.605	1.479	1.470	1.465	1.444	1.283	2.717	1.788	1.922	2.020
TS2c	PM3	1.534	1.439	1.492	1.462	1.574	1.222	2.751	1.889	2.078	2.216
	HF/3-21G	1.646	1.469	1.467	1.458	1.471	1.288	2.778	1.780	1.924	2.044
TS2d	PM3	1.882	1.397	1.483	1.429	1.348	1.559	2.896	1.781	2.016	2.166
TS2e	PM3	1.879	1.398	1.483	1.429	1.347	1.561	2.894	1.778	2.017	2.167
TS2f	PM3	1.909	1.394	1.481	1.429	1.349	1.604	2.886	1.793	2.012	2.204

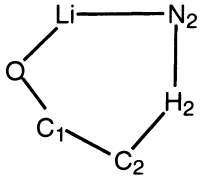

Scheme 3.

TS1a and **TS1b** differ mainly in the conformation of the cyclohexene oxide ring. In **TS1a** H_3 is positioned equatorially and $H_{3'}$ axially, while in **TS1b** $H_{3'}$ is equatorial and H_3 axial. Thus these hydrogens in **TS1b** adopt nearly eclipsed positions to H_2 and $H_{2'}$, respectively, while in **TS1a** H_3 and $H_{3'}$ are nearly staggered relative to H_2 and $H_{2'}$. The calculated energy difference between the two activated complexes (3.1 kcal mol^{-1}, favoring **TS1a**) reflects the differences in interactions described above.

No interaction between the axial H_4 in the cyclohexene oxide ring and H_7 in the lithium amide is detected in **TS1a**. The distance of 2.49 Å is larger than the sum of the van der Waal's radii of two hydrogens (2.40 Å). A distance of 2.32 Å is calculated between H_2 and $H_{15'}$ and also between H_7 and H_{12} in **TS1a** indicating only minor steric interactions. Also between **TS2a** and **TS2b** is the energy difference traced to the conformational difference between the cyclohexene oxide rings. Other interactions between the cyclohexene oxide ring and the lithium amide are small. A distance of 2.66 Å between H_3 and H_{15} and 2.25 Å between H_{10} and H_{12} is found in **TS2a**. In **TS1c** the cyclohexene oxide ring adopts the same conformation as in **TS1a** to eliminate the unfavorable eclipsing interactions.

An energy comparison of the TSs gives a difference of 0.81 kcal mol^{-1} in favor of **TS2a**, i.e. the TS yielding the (*S*)-alkoxide, over **TS1a** which yields the (*R*)-alkoxide (Table 2). After thermal and entropic corrections the difference in free energy at 298 K is calculated to be 0.82 kcal mol^{-1}. The small energy

Table 2
Calculated total energies (E) in a.u., relative activation energies ($\delta\Delta E^{\ddagger}$), and relative free activation energies ($\delta\Delta G^{\ddagger}$) in kcal mol^{-1} for deprotonation transition states

	E	$\delta\Delta E^{\ddagger}$	$\delta\Delta G^{\ddagger}$
HF/3-21G//HF/3-21G[1]			
TS1a	-770.62735	**0**	**0**
TS1b	-770.62245	+3.08	+2.65
TS1c	-770.62222	+3.22	+3.41
TS2a	-770.62865	**-0.81**	**-0.82**
TS2b	-770.62234	+3.14	+2.50
TS2c	-770.62373	+2.27	+2.22
B3LYP/6-31+G(d)//HF/3-21G			
TS1a	-780.09285	**0**	**0**
TS1b	-780.08756	+3.32	+2.90
TS1c	-780.08920	+2.29	+2.48
TS2a	-780.09417	**-0.83**	**-0.83**
TS2b	-780.08819	+2.92	+2.28
TS2c	-780.09263	+0.14	+0.09

1. Numbers in bold indicate the states with lowest energy

difference makes the interpretation intricate, but **TS2a** appears to have smaller steric interactions between the cyclohexene oxide ring and the lithium amide than **TS1a**. Thus this seems to be a major reason for the obtained enantioselectivity.

Single-point energy calculations using B3LYP/6-31+G(d) and HF/3-21G optimized geometry gave an energy difference of 0.83 kcal mol^{-1}. The difference in free energy at 298 K is calculated to be 0.83 kcal mol^{-1} at this level. This energy difference corresponds to an e.e. of 60% at 298 K.

TS1b and **TS1c** are calculated at the HF/3-21G level to be 3.1 and 3.2 kcal mol^{-1}, respectively, higher in energy than **TS1a**. The estimated corresponding differences in free energy are 2.7 and 3.4 kcal mol^{-1}, respectively. Single point energies at the B3LYP/6-31+G(d) level suggest these energies to be 3.3 and 2.3 kcal mol^{-1}, respectively, while the corresponding free energies are 2.9 and 2.5 kcal mol^{-1}, respectively. The corresponding energies for **TS2b** and **TS2c** are 3.1 and 2.3 kcal mol^{-1} at the HF/3-21G level and 2.9 and 0.1 kcal mol^{-1} at the B3LYP/6-31+G(d) level, respectively. The calculated free energies are 2.5 and 2.2 kcal mol^{-1} at the HF/3-21G level and 2.3 and 0.1 kcal mol^{-1} at the B3LYP/6-31+G(d) level. When using a correlated level for the energy calculation, **TS1c** and **TS2c** are energetically closer to **TS1a** and **TS2a**, while **TS1b** and **TS2b** remain essentially unaffected. No indication of any substantial Li–π interactions is found in the optimized structures.

3.2. Semiempirical structures and energies

PM3-optimized transition states for the epoxide opening are depicted in Fig. 4.

At the PM3 level, six transition states yielding the (*R*)-alkoxide and six yielding the (*S*)-alkoxide were identified. The structures **TS1d–f** and **TS2d–f** all feature long O–C_1 bonds. Attempts to optimize these

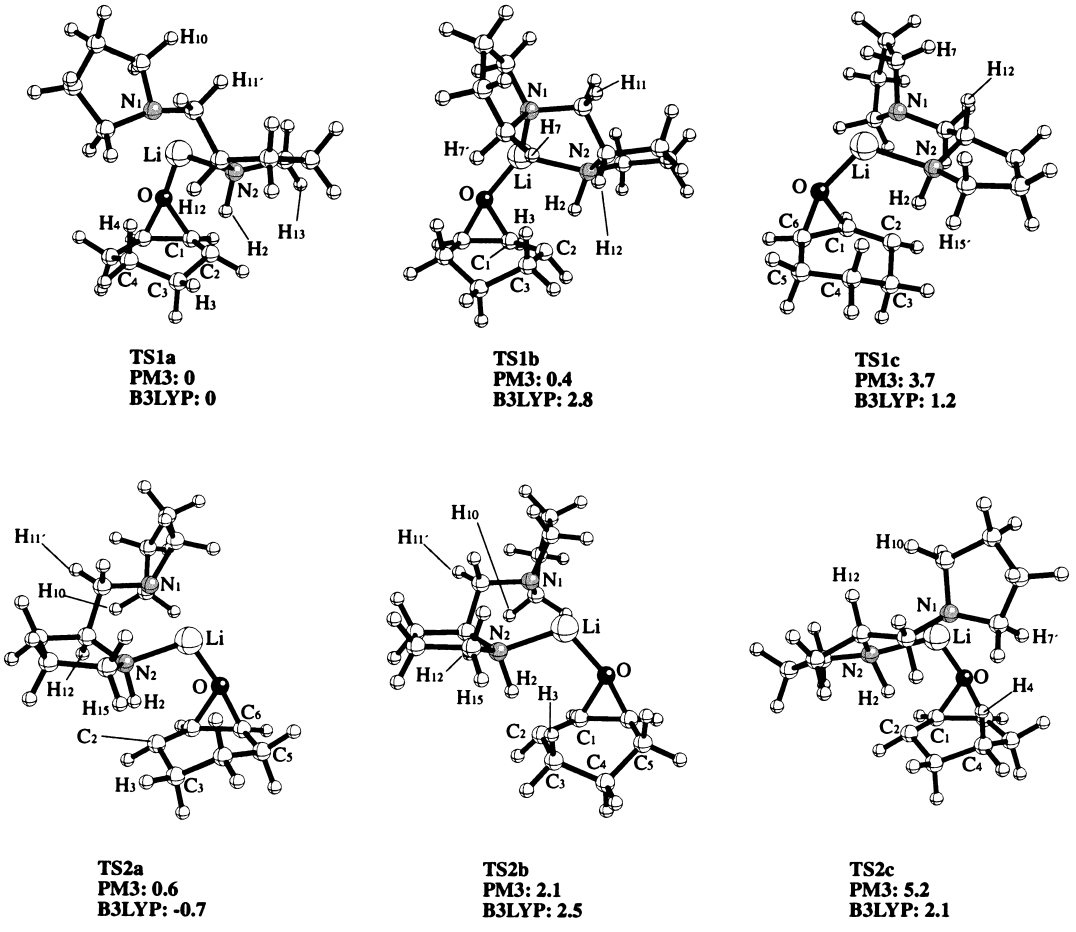

Figure 4. Calculated TSs for epoxide opening of cyclohexene oxide with **2** yielding (*R*)-alkoxide (**TS1a**–**c**) and (*S*)-alkoxide (**TS2a**–**c**)

states at the HF/3-21G level resulted only in the **TS1a**–**c** and **TS2a**–**c** structures, respectively. In the following discussion we have concentrated on the TSs present at both levels.

The epoxide rings in **TS1a**–**TS2c** at the PM3 level of theory are somewhat less opened than at the HF/3-21G level. O–C_1 distances are calculated to be 1.52–1.57 Å, with the longest bond found for **TS1c**, and O–C_6 distances are 1.43–1.44 Å. In **1** the O–C_1 distance is calculated to be 1.44 Å. The corresponding O–C bond distance in the lithium alkoxide of **3** is calculated to be 1.37 Å. Formation of the double bond is not complete in the TS. The bond distance between C_1 and C_2 is calculated to be 1.45–1.47 Å in **TS1a**–**TS2c**. In **3** the double bond is found to be 1.33 Å at the same level of theory. The proton in transit in **TS1a**–**TS2c** is *more* than half transferred towards the nitrogen, C_2–H_2 distances are 1.55–1.57 Å, and the proton transfer angle is 159–169°. The O–Li distances are calculated to be 1.86–1.89 Å in **TS1a**–**TS2c**, i.e. 0.1 Å longer than at the HF/3-21G level. The distance is also considerably longer than in **3** where the bond distance is found to be 1.60 Å. The lithium cation is also coordinating the amide nitrogen, N_2 (2.07–2.08 Å for **TS1a**–**TS2c**), and the amine nitrogen, N_1 (2.16–2.24 Å in all states), thus being tricoordinated. In the parent lithium amide, **2**, the corresponding bond distances are calculated to be 1.84 and 2.18 Å, respectively, at the same level of theory.

As in the HF/3-21G level of theory, the steric interactions at the PM3 level between the lithium amide and the cyclohexene oxide ring is small. In **TS1a** the H_2–H_{12} and H_2–H_{13} distances are 2.37 Å and the

distance between H_{10} and $H_{11'}$ is 2.23 Å. In **TS1b** the H_3–$H_{7'}$ distance is 2.57 Å and the H_7–H_{11} distance is 2.34 Å. Interactions between H_{10} and $H_{11'}$ (2.24 Å) and H_2–H_{12} (2.35 Å) are also found in **TS1b**. The eclipsed hydrogens in the cyclohexene oxide ring are in **TS1b** separated by 2.47 and 2.34 Å, respectively. In **TS1c** $H_{15'}$ is positioned 2.36 Å from H_2, indicating a small interaction, and the distance between H_{10} and $H_{11'}$ is found to be 2.25 Å. The lithium amide part adopts a different conformation in **TS1c** than in **TS1a**. The pyrrolidine ring is flipped and the dihedral angle C_{11}–C_{12}–C_{13}–C_{14} is found to be −151° in **TS1c**, compared to −118° in **TS1a** and **TS1b**. The adopted conformation of the lithium amide part results in some steric interactions between H_7 and H_{12}. The distance between the two hydrogens is calculated to be 2.30 Å which is slightly unfavorable. The energy difference between **TS1a** and **TS1b** is calculated to be 0.4 kcal mol^{-1}, while **TS1c** is 3.7 kcal mol^{-1} higher in energy than **TS1a**.

TS2a adopts a ring conformation without eclipsing hydrogens. H_3 and H_2 are separated by 2.53 Å and the distance between H_3 and H_{15} is found to be 2.51 Å. In **TS2b** the distance between the eclipsed hydrogens is 2.39 and 2.32 Å, respectively, and the distance between H_3 and H_{15} is 2.41 Å. In **TS2a–b**, H_{10}–$H_{11'}$ are interacting at the distance 2.23 Å, and H_2 interacts slightly with H_{12} at 2.38 Å. The sum of such interactions is assumed to be the origin of the higher energies of **TS2b** (+1.5 kcal mol^{-1}) over **TS2a**.

TS2c does not have any eclipsing hydrogens in the cyclohexene oxide ring and the pyrrolidine ring adopts a similar conformation as in **TS1c**, the dihedral angle C_{11}–C_{12}–C_{13}–C_{14} is found to be −154°. Also here are interactions between $H_{7'}$ and H_{12} detected by the distance 2.29 Å in **TS2c**.

In none of the optimized transition states at PM3 level could a strong Li–π interaction be detected. Li–C_1 distances were found to be about 2.9 Å, which is smaller than the sum of the van der Waals radius of a carbon and a lithium atom (3.5 Å), but indicates no direct coordination.

Comparison of the two lowest PM3-optimized transition states, **TS1a** and **TS2a**, shows that the energy difference is 0.5 kcal mol^{-1} in favor of the TS yielding the (*R*)-alkoxide which is contradictory to experiment and HF/3-21G calculations. PM3 is known to give reasonable structures while energies are not so well modeled. We therefore calculated the relative energies of **TS1a–c** and **TS2a–c** with B3LYP/6-31+G(d) and with PM3-optimized geometries to obtain more reliable energies. A difference of 0.7 kcal mol^{-1} in favor of the TS yielding the (*S*)-alkoxide was now found corresponding to an e.e. of 55% at 298 K. This method also predicts **TS1c** to be lower in energy than **TS1b**, and **TS2c** to be lower in energy than **TS2b**, which also was seen with HF/3-21G geometries using B3LYP energies. The steric interactions in the nearly eclipsed transition states seem to be underestimated in PM3.

Thus formation of an excess of the (*S*)-isomer is predicted in the absence of solvation at the highest level of theory used. The results obtained by also considering solvation of the activated complexes are presented in Table 3.

3.3. Solvation

Some computational studies on solvation in lithium organic chemistry at the semiempirical level can be found in the literature[49–56,27,57,58,23] but only sparsely at higher levels.[59–61]

In this work, the solvation was studied by direct coordination of one THF molecule to the lithium cation, thus making it tetracoordinated. The structures for the solvated complexes represent the most stable states achieved after a detailed investigation at the PM3 level of several local minima, obtained by solvent rotation around the Li–THF bond. Large energy variations were found depending on the arrangement of the solvent molecule.

Table 3
Calculated heats of formation (ΔH_f), absolute energies (E in a.u) and relative enthalpies ($\delta\Delta H_f$) in kcal mol^{-1} for deprotonation transition states

	ΔH_f	$\delta\Delta H_f$
PM3//PM3		
TS1a	-15.163	**0**
TS1b	-14.777	+0.39
TS1c	-11.420	+3.74
TS1d	-17.785	-2.62
TS1e	-13.715	+1.45
TS1f	-13.592	+1.57
TS2a	-14.614	**+0.55**
TS2b	-13.084	+2.08
TS2c	-9.944	+5.22
TS2d	-14.846	+0.32
TS2e	-13.396	+2.08
TS2f	-10.693	+4.47
B3LYP/6-31+G(d)//PM3	E	
TS1a	-780.07872	**0**
TS1b	-780.07424	+2.81
TS1c	-780.07675	+1.24
TS1d	-780.08577	-4.42
TS1e	-780.07808	+0.40
TS1f	-780.08389	-3.24
TS2a	-780.07988	**-0.73**
TS2b	-780.07479	+2.47
TS2c	-780.07545	+2.05
TS2d	-780.08586	-4.48
TS2e	-780.07883	-0.07
TS2f	-780.08185	-1.96

1. In a.u.

3.4. Semiempirical structures

Optimized solvated activated complexes for the epoxide opening are depicted in Fig. 5. Selected calculated bond distances of the optimized structures are presented in Table 4. Upon solvation, the changes in structure for the TSs are mainly found in the vicinity of the solvated lithium cation. For **TS1a–c** the O–Li bonds are elongated by 0.02–0.06 Å to 1.90–1.93 Å. **TS1a**+**THF** has the shortest and therefore the strongest O–Li bond. The Li–N_2 bonds are elongated by 0.03–0.04 Å to 2.09–2.11 Å and the Li–N_1 bonds are 0.03–0.05 Å longer than in the unsolvated structures. The position of the transferred hydrogen in **TS1a–c** is not greatly affected, only in **TS1a** is the N_2–H_2 bond shortened by 0.04 Å to 1.18 Å. The length of the O–C_1 distance is also somewhat shortened upon solvation, the distance is 0.01–0.04 Å shorter in the solvated states. The THF–Li distances are calculated to be 2.00–2.04 Å. The solvation energies differ in the three states. The solvation energy for **TS1c**+**THF** is 8.0 kcal mol^{-1} while for **TS1a**+**THF** and **TS1b**+**THF** it is 6.8 kcal mol^{-1} and 6.5 kcal mol^{-1}, respectively.

The solvated transition states giving the (*S*)-alkoxide, **TS2a–c**+**THF**, exhibit most of the features described for the transition states giving (*R*)-alkoxide. Li bonds to heteroatoms are elongated by 0.04–0.07 Å, however the degree of proton transfer is also only slightly affected in this case. The distance between the THF oxygen and Li is calculated to be 2.02 Å and the solvation energy ranges from 6.5 kcal mol^{-1} for **TS2c**+**THF** to 8.1 kcal mol^{-1} for **TS2b**+**THF**.

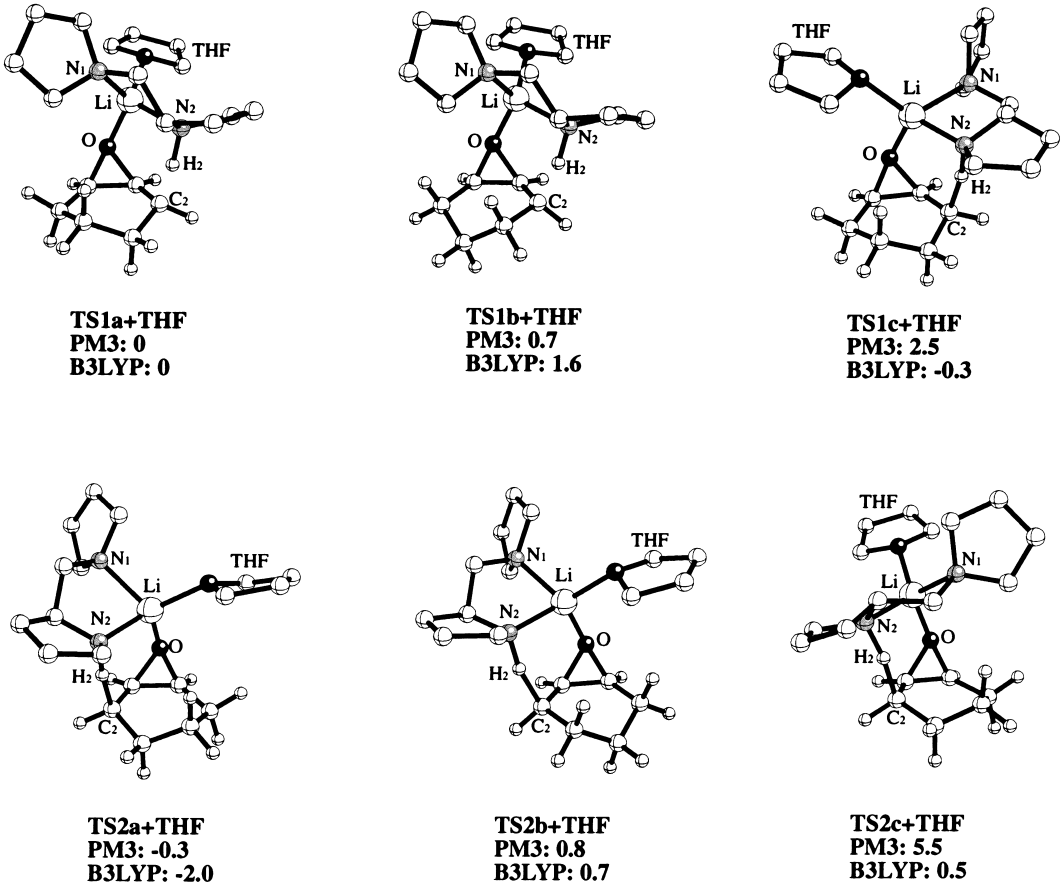

Figure 5. Calculated solvated TSs including solvent for epoxide opening of cyclohexene oxide with **2** yielding (*R*)-alkoxide and (*S*)-alkoxide. Some hydrogens are omitted for clarity

A comparison of the lowest transition states for yielding (*S*)- and (*R*)-alkoxide at this level indicates that solvation causes the energy differences in general to be larger. Solvation is somewhat more effective at this level of theory in the TSs yielding the (*S*)-alkoxide than the (*R*)-alkoxide. **TS2a**+**THF** is 0.3 kcal mol^{-1} lower in energy than **TS1a**+**THF** resulting in a predicted stereoselectivity in good agreement with experiment.

Single-point calculations at the B3LYP/6-31+G(d) level of theory with PM3-optimized geometries are also given in Table 5. **TS1c**+**THF** is the transition state with lowest energy yielding the (*R*)-alkoxide while **TS2a**+**THF** is the lowest TS for the (*S*)-route. The energy difference between the two TSs is 1.7 kcal mol^{-1}, corresponding to an e.e. of 88%, which is close to the experimental value of 80%. The solvation energies of **TS1a–c**+**THF** range from 9.1 kcal mol^{-1} for **TS1a**+**THF** to 10.7 kcal mol^{-1} for **TS1c**+**THF**. The solvation energies for **TS2a–c**+**THF** vary from 10.4 kcal mol^{-1} for **TS2a**+**THF** to 11.0 kcal mol^{-1} for **TS2b**+**THF**.

To improve the energies of the solvated transition states we optimized the key structures with the ab initio method HF/3-21G.

3.5. Ab initio structures

Optimized transition states are shown in Fig. 6 while selected bond distances are given in Table 4.

Table 4. Selected calculated bond distances (Å) at PM3 and HF/3-21G levels of theory for solvated deprotonation transition states

	Method	O-C_1	O-C_6	C_1-C_6	C_1-C_2	C_2-H_2	N_2-H_2	C_2-N_2	O-Li	Li-N_2	Li-N_1	Li-THF
TS1a+THF	PM3	1.545	1.434	1.491	1.451	1.555	1.178	2.718	1.896	2.113	2.206	1.998
	HF/3-21G	1.605	1.472	1.469	1.465	1.440	1.287	2.723	1.888	1.990	2.089	1.946
TS1b+THF	PM3	1.512	1.441	1.496	1.463	1.546	1.209	2.736	1.919	2.109	2.192	2.029
TS1c+THF	PM3	1.531	1.437	1.492	1.456	1.546	1.215	2.751	1.930	2.094	2.262	2.012
TS2a+THF	PM3	1.519	1.439	1.494	1.461	1.539	1.215	2.744	1.934	2.101	2.201	2.018
	HF/3-21G	1.600	1.473	1.470	1.467	1.439	1.283	2.719	1.884	1.987	2.083	1.923
TS2b+THF	PM3	1.509	1.442	1.496	1.463	1.539	1.217	2.737	1.927	2.111	2.216	2.024
TS2c+THF	PM3	1.524	1.438	1.492	1.461	1.558	1.230	2.745	1.926	2.100	2.268	2.020

Table 5
Calculated heats of formation (ΔH_f), absolute energies (E in a.u.), relative enthalpies ($\delta\Delta H_f$) and solvation energies (E_{sol}) in kcal mol^{-1} for solvated deprotonation transition states

	ΔH_f	$\delta\Delta H_f$	E_{sol}
PM3//PM3			
TS1a+THF[1]	-73.034	**0**	6.76
TS1b+THF	-72.362	+0.67	6.47
TS1c+THF	-70.529	+2.51	7.99
TS2a+THF	-73.307	**-0.27**	7.56
TS2b+THF	-72.272	+0.76	8.07
TS2c+THF	-67.523	+5.51	6.46
B3LYP/6-31+G(d)//PM3	E		
TS1a+THF[2]	-1012.54696	0	9.16
TS1b+THF	-1012.54440	+1.61	10.37
TS1c+THF	-1012.54747	**-0.32**	10.72
TS2a+THF	-1012.55013	**-1.99**	10.42
TS2b+THF	-1012.54591	+0.66	10.97
TS2c+THF	-1012.54622	+0.46	10.75

1. THF=-51.115 kcal mol^{-1} 2. THF=-232.45364 a.u.

The non-solvent parts of the HF/3-21G optimized structures differ somewhat from the unsolvated structures. The largest effect is seen in the vicinity of the lithium. The O–Li distance is shortened by 0.01 Å in **TS1a** and by 0.05 Å in **TS2a**. Similarly, the Li–N_2 and Li–N_1 distances are shortened by 0.12 Å for both structures. The N_2–H_2 distance also shows some dependence upon solvation; the distance is elongated by 0.11 Å in **TS1a** and 0.07 Å in **TS2a**. The distance between Li and O in THF is calculated to be 1.92–1.95 Å at this level of theory.

Calculated energies at the HF/3-21G//HF/3-21G level of theory show that **TS2a**+**THF** is 2.21 kcal mol^{-1} lower in energy than **TS1a**+**THF** (Table 6). The corresponding difference in free energy is 1.96 kcal mol^{-1}. Single point calculations at this geometry using B3LYP/6-31+G(d) do not change the relative energies much, i.e. **TS2a**+**THF** is 2.23 kcal mol^{-1} lower in energy and 1.98 kcal mol^{-1} lower in free energy. This is 0.7 kcal mol^{-1} larger than the experimental value but the stereoselectivity has the correct sign. The enantiomeric excess of the reaction at this level is calculated to be 93%. The solvation energy seems to be overestimated at the HF/3-21G level (−20.2 kcal mol^{-1} for **TS2a**+**THF** and −18.0 kcal mol^{-1} for **TS1a**+**THF**). At the B3LYP/6-31+G(d) level, the corresponding solvation energies are 8.5 and 7.1 kcal mol^{-1}, respectively, i.e. the TS giving the (*S*)-alkoxide is better solvated by THF.

4. Conclusion

A detailed computational investigation of possible activated complexes in the epoxide opening of cyclohexene oxide by a chiral lithium amide has been presented. Transition states for the two routes

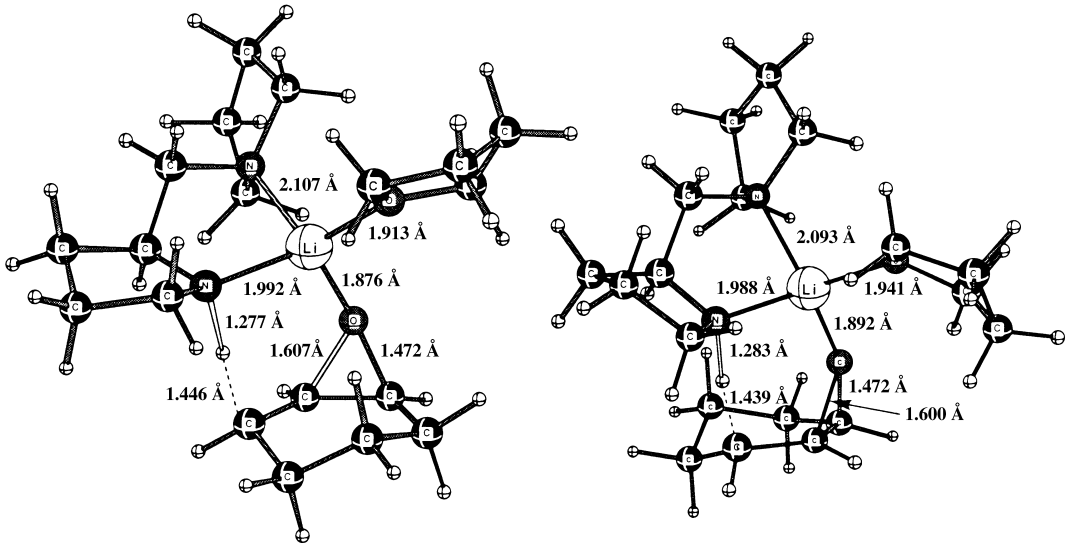

Figure 6. Calculated (HF/3-21G//HF/3-21G) solvated TSs for epoxide opening of cyclohexene oxide with **2** yielding (*R*)-alkoxide and (*S*)-alkoxide

Table 6
Calculated total energies (E) in a.u., solvation energies (E_{sol}), relative activation energies ($\delta\Delta E^{\ddagger}$) and relative free activation energies ($\delta\Delta G^{\ddagger}$) in kcal mol^{-1} for solvated deprotonation transition states

	E	E_{sol}	$\delta\Delta E^{\ddagger}$	$\delta\Delta G^{\ddagger}$
HF/3-21G//HF/3-21G				
TS1a+THF[1]	-1000.35526	-18.0	0	0
TS1c+THF	-1000.35454		0.45	
TS2a+THF	-1000.35878	-20.2	-2.21	-1.96
B3LYP/6-31+G(d)//HF/3-21G				
TS1a+THF[2]	-1012.56188	-7.10	0	0
TS1c+THF	-1012.56166		0.14	
TS2a+THF	-1012.56544	-8.50	-2.23	-1.98

1. THF= -229.69916 a.u.

2. THF= -232.45772 a.u.

giving (*S*)- and (*R*)-alkoxide with and without solvent, respectively, have been calculated. Geometry optimizations at the PM3 and HF/3-21G levels of theory, and single point calculations at the B3LYP/6-31+G(d) level have been used. PM3 itself does not reproduce even qualitatively the stereoselectivity for the reaction in the unsolvated case. At the B3LYP/6-31+G(d)//PM3 level, the (*S*)-transition state is favored by 0.7 kcal mol^{-1} (55% e.e.), and the observed stereoselectivity is also qualitatively reproduced at the HF/3-21G level. The difference in free activation energy is calculated to be 0.8 kcal mol^{-1} (60% e.e.) at the B3LYP/6-31+G(d)//HF/3-21G level, which is to be compared with 1.2 kcal mol^{-1} (80% e.e.) found experimentally. Upon inclusion of solvation by THF, the correct stereoselectivity is semi-quantitatively predicted at both PM3 and HF/3-21G levels. The free activation energy is calculated to be 2.0 kcal mol^{-1} (93% e.e.) at the B3LYP/6-31+G(d)//HF/3-21G level, favoring the transition state giving the (*S*)-alkoxide, while at the B3LYP/6-31+G(d)//PM3 level, the difference is found to be 1.7 kcal mol^{-1} (88% e.e.). Thus the observed stereoselectivity is semi-quantitatively reproduced at all levels except in the unsolvated case at PM3//PM3. Important factors controlling the stereoselectivity (other than those previously proposed) are solvation, which is larger in the TS yielding the (*S*)-alkoxide, and small differences in steric interactions between the cyclohexene oxide ring and the lithium amide in the activated complexes.

References

1. Asami, M. *Chem. Lett*. **1984**, 829.
2. Asami, M. *Tetrahedron Lett*. **1985**, *26*, 5803.
3. Asami, M.; Kirihara, H. *Chem. Lett*. **1987**, 389.
4. Hendrie, S. K.; Leonard, J. *Tetrahedron* **1987**, *43*, 3289.
5. Asami, M. *Bull. Chem. Soc. Jpn*. **1990**, *63*, 721.
6. Asami, M. *Bull. Chem. Soc. Jpn*. **1990**, *63*, 1402.
7. Leonard, J.; Hewitt, J. D.; Ouali, D.; Simpson, S. J.; Newton, R. F. *Tetrahedron Lett*. **1990**, *31*, 6703.
8. Cox, P. J.; Simpkins, N. S. *Tetrahedron: Asymmetry* **1991**, *2*, 1.
9. Asami, M.; Ishizaki, T.; Inoue, S. *Tetrahedron: Asymmetry* **1994**, *5*, 793.
10. Asami, M.; Takahashi, J.; Inoue, S. *Tetrahedron: Asymmetry* **1994**, *5*, 1649.
11. Bhuniya, D.; Singh, V. K. *Synth. Commun*. **1994**, *24*, 375.
12. Bhuniya, D.; Singh, V. K. *Synth. Commun*. **1994**, *24*, 1475.
13. Asami, M.; Inoue, S. *Tetrahedron* **1995**, *51*, 11725.
14. Bhuniya, D.; DattaGupta, A.; Singh, V. K. *Tetrahedron Lett*. **1995**, *36*, 2847.
15. Asami, M. *J. Synth. Org. Chem. Jpn*. **1996**, *54*, 188.
16. Bhuniya, D.; DattaGupta, A.; Singh, V. K. *J. Org. Chem*. **1996**, *61*, 6108.
17. Hodgson, D. M.; Gibbs, A. R. *Tetrahedron: Asymmetry* **1996**, *7*, 407.
18. Hodgson, D. M.; Gibbs, A. R.; Lee, G. P. *Tetrahedron* **1996**, *52*, 14361.
19. Khan, A. Z.-Q.; Arvidsson, P. I.; Ahlberg, P. *Tetrahedron: Asymmetry* **1996**, *7*, 399.
20. Morgan, K. M.; Gajewski, J. J. *J. Org. Chem*. **1996**, *61*, 820.
21. O'Brien, P.; Poumellec, P. *Tetrahedron Lett*. **1996**, *37*, 8057.
22. Asami, M.; Suga, T.; Honda, K.; Inoue, S. *Tetrahedron Lett*. **1997**, *38*, 6425.
23. Hilmersson, G.; Arvidsson, P. I.; Davidsson, Ö.; Håkansson, M. *Organometallics* **1997**, *16*, 3352.
24. Tierney, J. P.; Alexakis, A.; Mangeney, P. *Tetrahedron: Asymmetry* **1997**, *8*, 1019.
25. O'Brien, P. *J. Chem. Soc., Perkin Trans. 1* **1998**, 1439.
26. Södergren, M. J.; Andersson, P. G. *J. Am. Chem. Soc*. **1998**, *120*, 10760.
27. Mück-Lichtenfeld, C.; Ahlbrecht, H. *Tetrahedron* **1996**, *52*, 10025.
28. Pratt, L. M.; Khan, I. M. *Tetrahedron: Asymmetry* **1996**, *6*, 2165.
29. Abbotto, A.; Streitwieser, A.; Schleyer, P. v. R. *J. Am. Chem. Soc*. **1997**, *119*, 11255.
30. Hoppe, D.; Hense, T. *Angew. Chem., Int. Ed. Engl*. **1997**, *36*, 2282.
31. Arvidsson, P. I.; Ahlberg, P.; Hilmersson, G. *Eur. J. Chem.*, in press.

32. Arvidsson, P. I.; Hansson, M.; Khan, A. Z.-Q.; Ahlberg, P. *Can. J. Chem*. **1998**, 795.
33. Arvidsson, P. I.; Hilmersson, G.; Ahlberg, P. *J. Am. Chem. Soc*., in press.
34. Nilsson Lill, S. O.; Arvidsson, P.; Ahlberg, P. *Acta. Chem. Scand*. **1998**, *52*, 280.
35. Gaussian 94, Rev. D3; Frisch, M. J.; Trucks, G. W.; Schlegel, H. B.; Gill, P. M. W.; Johnson, B. G.; Robb, M. A.; Cheeseman, J. R.; Keith, T.; Petersson, G. A.; Montgomery, J. A.; Raghavachari, K.; Al-Laham, M. A.; Zakrzewski, V. G.; Ortiz, J. V.; Foresman, J. B.; Cioslowski, J.; Stefanov, B. B.; Nanayakkara, A.; Challacombe, M.; Peng, C. Y.; Ayala, P. Y.; Chen, W.; Wong, M. W.; Andres, J. L.; Replogle, E. S.; Gomperts, R.; Martin, R. L.; Fox, D. J.; Binkley, J. S.; Defrees, D. J.; Baker, J.; Stewart, J. P.; Head-Gordon, M.; Gonzales, C.; Pople, J. A. Gaussian Inc.: Pittsburgh, PA, 1995.
36. Spartan v. 5.0.1; Hehre, W. J.; Deppmeier, B. J.; Driessen, A. J.; Johnson, J. A.; Klunzinger, P. E.; Lou, L.; Yu, J.; Baker, J.; Carpenter, J. E.; Dixon, R. W.; Fielder, S. S.; Johnson, H. C.; Kahn, S. D.; Leonard, J. M.; Pietro, W. J. Wavefunction Inc.: Irvine, CA, 1997.
37. Stewart, J. J. *J. Comput. Chem*. **1989**, *10*, 209.
38. Anders, E.; Koch, R.; Freunscht, P. *J. Comput. Chem*. **1993**, *14*, 1301.
39. Binkley, J. S.; Pople, J. A.; Hehre, W. J. *J. Am. Chem. Soc*. **1980**, *102*, 939.
40. Huang, W., personal communication.
41. Csonka, G. I. *J. Comp. Chem*. **1993**, *14*, 895.
42. Francl, M. M.; Pietro, W. J.; Hehre, W. J.; Binkley, J. S.; Gordon, M. S.; DeFrees, D. J.; Pople, J. A. *J. Chem. Phys*. **1982**, *77*, 3654.
43. Spitznagel, G. W.; Clark, T.; Chandrasekhar, J.; Schleyer, P. v. R. *J. Comput. Chem*. **1982**, *3*, 363.
44. Becke, A. D. *J. Chem. Phys*. **1994**, *98*, 5648.
45. Thummel, R. P.; Rickborn, B. *J. Am. Chem. Soc*. **1970**, *92*, 2064.
46. Pawar, D. M.; Noe, E. A. *J. Am. Chem. Soc*. **1998**, *120*, 1485.
47. Curtin, D. Y. *Rec. Chem. Progr*. **1954**, *15*, 111.
48. Hammett, L. P. *Physical Organic Chemistry*; 2nd edn; McGraw-Hill: New York, 1970.
49. Kaufmann, E.; Raghavachari, K.; Reed, A.; Schleyer, P. v. R. *Organometallics* **1988**, *7*, 1597.
50. Boche, G.; Fraenkel, G.; Cabral, J.; Harms, K.; van Eikemma Hommes, N. J. R.; Lohrenz, J.; Marsch, M.; Schleyer, P. v. R. *J. Am. Chem. Soc*. **1992**, *114*, 1562.
51. Romesberg, F. E.; Collum, D. B. *J. Am. Chem. Soc*. **1992**, *114*, 2112.
52. Anders, E.; Opitz, A.; van Eikema Hommes, N. J. R.; Hampel, F. *J. Org. Chem*. **1993**, *58*, 4424.
53. Romesberg, F. E.; Collum, D. B. *J. Am. Chem. Soc*. **1994**, *116*, 9187.
54. Lucht, B. L.; Collum, D. B. *J. Am. Chem. Soc*. **1995**, *117*, 9863.
55. Romesberg, F. E.; Collum, D. B. *J. Am. Chem. Soc*. **1995**, *117*, 2166.
56. Koch, R.; Wiedel, A.; Anders, E. *J. Org. Chem*. **1996**, *61*, 2523.
57. Sorger, K.; Schleyer, P. v. R.; Fleischer, R.; Stalke, D. *J. Am. Chem. Soc*. **1996**, *118*, 6924.
58. Weiss, H.; Yakimansky, A. V.; Müller, A. H. E. *J. Am. Chem. Soc*. **1996**, *118*, 8897.
59. Sapse, A. M.; Jain, D. C. *J. Phys. Chem*. **1987**, *91*, 3923.
60. Kaufmann, E.; Gose, J.; Schleyer, P. v. R. *Organometallics* **1989**, *8*, 2577.
61. Glaser, R.; Streitwieser, A. *J. Org. Chem*. **1991**, *56*, 6612.